Search for heavy neutral leptons using tau lepton decays at *BABAR*

J. P. Lees, V. Poireau, V. Tisserand, E. Grauges, A. Palano, G. Eigen, D. N. Brown, Yu. G. Kolomensky, M. Fritsch, H. Koch, R. Cheaib, C. Hearty, T. S. Mattison, J. A. McKenna, R. Y. So, V. E. Blinov, A. R. Buzykaev, V. P. Druzhinin, E. A. Kozyrev, E. A. Kravchenko, S. I. Serednyakov, Yu. I. Skovpen, E. P. Solodov, K. Yu. Todyshev, A. J. Lankford, B. Dey, J. W. Gary, O. Long, A. M. Eisner, W. S. Lockman, W. Panduro Vazquez, D. S. Chao, C. H. Cheng, B. Echenard, K. T. Flood, D. G. Hitlin, Y. Li, D. X. Lin, S. Middleton, T. S. Miyashita, P. Ongmongkolkul, J. Oyang, F. C. Porter, M. Röhrken, B. T. Meadows, M. D. Sokoloff, J. G. Smith, S. R. Wagner, D. Bernard, M. Verderi, D. Bettoni, C. Bozzi, R. Calabrese, G. Cibinetto, E. Fioravanti, I. Garzia, E. Luppi, V. Santoro, A. Calcaterra, R. de Sangro, G. Finocchiaro, S. Martellotti, P. Patteri, I. M. Peruzzi, M. Piccolo, M. Rotondo, A. Zallo, S. Passaggio, C. Patrignani, B. J. Shuve, H. M. Lacker, B. Bhuyan, U. Mallik, C. Chen, J. Cochran, S. Prell, A. V. Gritsan, N. Arnaud, M. Davier, F. Le Diberder, A. M. Lutz, G. Wormser, D. J. Lange, D. M. Wright, J. P. Coleman, D. E. Hutchcroft, D. J. Payne, C. Touramanis, A. J. Bevan, F. Di Lodovico, G. Cowan, Sw. Banerjee, D. N. Brown, C. L. Davis, A. G. Denig, W. Gradl, K. Griessinger, A. Hafner, K. R. Schubert, R. J. Barlow, G. D. Lafferty, R. Cenci, A. Jawahery, D. A. Roberts, R. Cowan, S. H. Robertson, R. M. Seddon, N. Neri, F. Palombo, L. Cremaldi, R. Godang, D. J. Summers,* G. De Nardo, C. Sciacca, C. P. Jessop, J. M. LoSecco, K. Honscheid, A. Gaz, M. Margoni, G. Simi, F. Simonetto, R. Stroili, S. Akar, E. Ben-Haim, M. Bomben, G. R. Bonneaud, G. Calderini, J. Chauveau, G. Marchiori, J. Ocariz, M. Biasini, E. Manoni, A. Rossi, G. Batignani, S. Bettarini, M. Carpinelli, G. Casarosa, M. Chrzaszcz, F. Forti, M. A. Giorgi, A. Lusiani, B. Oberhof, E. Paoloni, M. Rama, G. Rizzo, J. J. Walsh, L. Zani, A. J. S. Smith, F. Anulli, R. Faccini, F. Ferrarotto, F. Ferroni, A. Pilloni, C. Bünger, S. Dittrich, O. Grünberg, T. Leddig, C. Voß, R. Waldi, T. Adye, F. F. Wilson, S. Emery, G. Vasseur, D. Aston, C. Cartaro, M. R. Convery, M. Ebert, R. C. Field, B. G. Fulsom, M. T. Graham, C. Hast, P. Kim, S. Luitz, D. B. MacFarlane, D. R. Muller, H. Neal, B. N. Ratcliff, A. Roodman, M. K. Sullivan, J. Va'vra, W. J. Wisniewski, M. V. Purohit, J. R. Wilson, S. J. Sekula, H. Ahmed, N. Tasneem, M. Bellis, P. R. Burchat, E. M. T. Puccio, J. A. Ernst, R. Gorodeisky, N. Guttman, D. R. Peimer, A. Soffer, S. M. Spanier, J. L. Ritchie, J. M. Izen, X. C. Lou, F. Bianchi, F. De Mori, A. Filippi, L. Lanceri, L. Vitale, F. Martinez-Vidal, A. Oyanguren, J. Albert, A. Beaulieu, F. U. Bernlochner, G. J. King, R. Kowalewski, T. Lueck, C. Miller, I. M. Nugent, J. M. Roney, R. J. Sobie, T. J. Gershon, P. F. Harrison, T. E. Latham, and S. L. Wu

(The *BABAR* Collaboration)

(Received 21 July 2022; accepted 13 September 2022; published 23 March 2023)

This article presents a model-independent search for an additional, mostly sterile, heavy neutral lepton (HNL), that is capable of mixing with the Standard Model τ neutrino with a mixing strength of $|U_{\tau 4}|^2$, corresponding to the absolute square of the extended Pontecorvo-Maki-Nakagawa-Sakata matrix element. Data from the *BABAR* experiment, with a total integrated luminosity of 424 fb^{-1}, are analyzed using a kinematic approach that makes no assumptions on the model behind the origins of the HNL, its lifetime or decay modes. No significant signal is found. Upper limits on $|U_{\tau 4}|^2$ at the 95% confidence level, depend on the HNL mass hypothesis and vary from 2.31×10^{-2} to 5.04×10^{-6} (with all uncertainties considered), across the mass range $100 < m_4 < 1300$ MeV$/c^2$; the more stringent limits being placed at higher masses.

DOI: 10.1103/PhysRevD.107.052009

*Deceased

I. MOTIVATIONS

Heavy neutral leptons (HNLs) are predicted by many extensions of the Standard Model (SM) to explain several phenomena. They interact via gravity but have no electric charge, no weak hypercharge, no weak isospin, and no color charge; HNLs have no ordinary weak interactions,

except those induced by mixing. They are generally considered singlets under all gauge interactions and are often referred to as "sterile neutrinos." A theoretical overview and experimental review of recent searches for HNLs can be found in Refs. [1,2].

Observation of neutrino oscillations has established the nonzero mass of at least two of the SM neutrinos. Absolute values of these masses are yet to be determined, but experiments have measured the mass squared differences, with current bounds detailed in Ref. [3]. Sterile neutrinos have long been used to explain the apparent smallness of the SM neutrino masses [4].

Heavy neutral leptons could also be responsible for the generation of the matter-antimatter asymmetry of the Universe [5] via leptogenesis [6,7]. Leptogenesis scenarios can predict HNLs at a mass scale as low as $\mathcal{O}(\mathrm{GeV}/c^2)$ [8], thus these theories can be explored in current, and near-future, particle physics experiments.

The neutrino minimal standard model (or ν-MSM) [9] is one theory that predicts HNLs at the GeV/c^2 scale. In ν-MSM adding three sterile, right-handed, Majorana HNLs to the SM can explain neutrino oscillations, the origin of the baryon asymmetry of the Universe [9,10], and provide a dark matter candidate [11]. Two of these HNLs have masses in the MeV/c^2 to GeV/c^2 range and a third, the dark matter candidate, has mass at the keV/c^2 scale. The ν-MSM is compatible with all current measurements.

Sterile fermions of masses $\mathcal{O}(\mathrm{eV}/c^2)$ can also explain the anomalies in very short baseline oscillation measurements and cosmological data analyses [12]. Recent reanalysis of data from the GALLEX [13] and SAGE [14] solar neutrino experiments has exposed an unexplained $14 \pm 5\%$ deficit in the number of recorded ν_e; referred to as the "gallium anomaly." In addition, numerous analyses of the flux of $\bar{\nu}_e$ from reactors have suggested a deficit of $\bar{\nu}_e$ at the 98.6% confidence level (CL) [15]; denoted as the "reactor antineutrino anomaly." A third anomaly—the "accelerator anomaly"—stems from measurements at the LSND [16] experiment that evaluated the oscillation $\nu_e \to \nu_\mu$ at a baseline of $L = 30$ m. The LSND experiment measured an excess of neutrinos at the level of 3.8σ, which could be explained by the existence of a sterile neutrino with a mass $\mathcal{O}(\mathrm{eV}/c^2)$. Further support for this excess was presented by the MiniBooNE experiment at the 2.8σ level [17], although recent results from MicroBooNE do not yet support this anomaly [18].

Heavy neutral leptons with mass in the MeV/c^2 to GeV/c^2 range could be produced in τ decays, giving rise to deviations from the SM expectations. In this article the possibility of an additional neutrino state (associated with the HNL) interacting with the τ-lepton, via charged-current weak interactions, is considered. Mixing between the HNL mass eigenstate and the active neutrinos can be parametrized by the extended Pontecorvo-Maki-Nakagawa-Sakata (PMNS) matrix with additional elements U_{l4}, where l denotes the SM lepton flavor state i.e. e, μ, τ

$$\begin{pmatrix} \nu_e \\ \nu_\mu \\ \nu_\tau \\ \nu_{\mathrm{L}} \end{pmatrix} = \begin{pmatrix} U_{e1} & U_{e2} & U_{e3} & U_{e4} \\ U_{\mu 1} & U_{\mu 2} & U_{\mu 3} & U_{\mu 4} \\ U_{\tau 1} & U_{\tau 2} & U_{\tau 3} & U_{\tau 4} \\ U_{\mathrm{L}1} & U_{\mathrm{L}2} & U_{\mathrm{L}3} & U_{\mathrm{L}4} \end{pmatrix} \begin{pmatrix} \nu_1 \\ \nu_2 \\ \nu_3 \\ \nu_4 \end{pmatrix},$$

where L represents some hypothetical additional lepton flavor. Analyses of cosmological data and Z boson decays, summarized in Ref. [3], are consistent with there being only three charged lepton flavors. Here, the PMNS matrix is extended for just one HNL, but others can be added in the same way. The PMNS matrix for the antineutrinos is identical to that for neutrinos under CPT symmetry. Experimental data on the mixing strength between the τ sector and a HNL are limited. Although the probability of a fourth neutrino state interacting with the electron ($|U_{e4}|^2$) or muon ($|U_{\mu 4}|^2$) has tight constraints [3], limits on $|U_{\tau 4}|^2$ are weaker, motivating the possibility that $|U_{\tau 4}| \gg |U_{e4}|$, $|U_{\mu 4}|$. In this article a search for a HNL with mass in the range $100\ \mathrm{MeV}/c^2 < m_4 < 1300\ \mathrm{MeV}/c^2$ is presented. Existing bounds in the range $\sim 300\ \mathrm{MeV}/c^2$ to $\sim 1\ \mathrm{GeV}/c^2$ range are particularly weak.

II. CURRENT BOUNDS

Numerous experiments have searched for the existence of HNLs with mass from $\mathcal{O}(\mathrm{eV}/c^2)$ up to hundreds of GeV/c^2, with no evidence seen.

Robust bounds on the mixing of heavy neutrinos with both electron and muon neutrinos have been provided by searches for excesses in the missing mass distribution of pions and kaons leptonic decays. Strong constraints on couplings have already been set by several experiments, such as PS191 [19], Charm [20], NuTeV [21], E949 [22], PIENU [23], TRIUMF-248 [24], NA3 [25], and NA62 [26]. MicroBooNe has also recently placed new limits on the mixing in the muon sector [27,28].

The current limits on $|U_{\tau 4}|^2$ come from the Nomad [29], Charm [20], and Delphi [30] experiments. More recently ArgoNeuT published limits [31] in the 280–970 MeV/c^2 range through a search for a Dirac HNL decaying to $\nu\mu^+\mu^-$. The Charm experiment conducted a search for HNLs produced in the decay of neutral particles into two electrons and provided limits on $|U_{\tau 4}|^2$ in the mass range 10–290 MeV/c^2. The Nomad experiment collected 4.1×10^{19} 450 GeV protons on target at the WANF facility at CERN. A search for $D_s \to \tau\nu_R$ followed by $\nu_R \to \nu_\tau e^+ e^-$ was conducted, resulting in an upper limit on $|U_{\tau 4}|^2$ in the mass range from 10–190 MeV/c^2. The Delphi experiment at LEP provided limits on $|U_{\tau 4}|^2$ in the GeV/c^2 mass range through searching for signatures of HNLs decaying to visible SM particles, specifically $e^+e^- \to Z \to \nu\nu_4$.

In Ref. [32] the τ and meson branching ratios are used to further constrain the parameter space.

III. DATA SAMPLE AND DETECTOR

The data sample used in this analysis corresponds to an integrated luminosity of 424 fb^{-1} [33], collected with the *BABAR* detector at the PEP-II e^+e^- storage ring at the SLAC National Accelerator Laboratory. At PEP-II, 9 GeV electrons collide with 3.1 GeV positrons at c.m. energies near 10.58 GeV, on the $\Upsilon(4S)$ resonance; 10% of the data were recorded 40 MeV below this resonance. The average cross section for τ-pair production of electron-positron annihilation is $\sigma(e^+e^- \to \tau^+\tau^-) = (0.919 \pm 0.003)$ nb [3]; thus the data sample corresponds to $\sim 4 \times 10^8$ produced τ-pairs, before applying any reconstruction or selection criteria.

In the *BABAR* detector [34,35] a silicon vertex tracker (SVT) and a 40 layer drift chamber (DCH), placed inside a 1.5-T solenoid magnet, are utilized to reconstruct charged-particle tracks. The transverse momentum resolution is 0.47% at 1 GeV/c, where the transverse momentum, p_T, is defined as the total momentum of all four tracks orthogonal to the beam axis.

An electromagnetic calorimeter (EMC) measures the energy of electrons and photons with a resolution of 3% at 1 GeV. A ring-imaging Cherenkov detector (DIRC) is located in front of the EMC and is used, together with specific ionization loss measurements in the SVT and DCH, to identify charged pions and kaons, and provide additional electron identification. The instrumented flux return of the solenoid is used to identify muons.

IV. EXPERIMENTAL STRATEGY

The analysis approach in this study was originally proposed in Ref. [36] and follows from that used by ALEPH to attempt to determine the τ neutrino mass [37]. We consider that HNL can interact with the tau via charged-current weak interactions. The key principle is that if the decay products of the τ have recoiled against a heavy neutrino, the phase space and the kinematics of the visible particles would be modified with respect to SM τ decay with a massless neutrino. We assume that the HNL does not decay within the detector.

This search studies the 3-prong, pionic τ decay since it has a relatively large branching fraction and gives access to the region $300 < m_4 < 1360$ MeV/c^2 (up to the kinematic endpoint), which historically has weaker constraints, whilst pion channels of higher multiplicity would only test the lower-mass region that is already well-constrained. It should be noted that the mass of the SM τ neutrino is unknown and the current upper limit on the heaviest neutrino is <18.2 [95% confidence level (CL)] MeV/c^2 [3]. In this analysis all SM neutrinos are assumed to have zero mass; changing the SM neutrino masses from 0 to the experimental upper limit induces negligible changes in the kinematic distributions used.

The 3-prong decay can be considered a 2 body decay,

$$\tau^- \to h^-(E_h, \vec{p}_h) + \nu(E_\nu, \vec{p}_\nu), \tag{1}$$

where h^- denotes the hadronic system and ν describes the outgoing neutrino state. An analogous equation could be written for the τ^+ channel. The allowed phase space of the reconstructed energy, E_h, and invariant mass, m_h, of the hadronic system would vary as functions of the mass of the HNL. As the HNL gets heavier the proportion of the original τ lepton's energy going to the visible pions diminishes.

In the c.m. frame the τ-lepton energy is assumed to be $\sqrt{s}/2$, when there is no initial state radiation. Since the direction of the decaying τ lepton is not known we cannot compute the neutrino mass directly but we know that E_h must fall between two extremes that define the kinematically allowed values,

$$E_\tau - \sqrt{m_4^2 + q_+^2} < E_h < E_\tau - \sqrt{m_4^2 + q_-^2}, \tag{2}$$

where

$$q_\pm = \frac{m_\tau}{2}\left(\frac{m_h^2 - m_\tau^2 - m_4^2}{m_\tau^2}\right)\sqrt{\frac{E_\tau^2}{m_\tau^2} - 1} \pm \frac{E_\tau}{2}\sqrt{\left(1 - \frac{(m_h + m_4)^2}{m_\tau^2}\right)\left(1 - \frac{(m_h - m_4)^2}{m_\tau^2}\right)}, \tag{3}$$

and $3m_{\pi^\pm} < m_h < m_\tau - m_4$. As the HNL mass increases, the allowed phase space of the visible system is reduced in the $E_h - m_h$ plane.

The observed kinematic phase space distributions of the hadronic system could be assumed to be a superposition of two phase spaces; the one associated with the heavy neutrino (weighted by $|U_{\tau 4}|^2$), and that associated with a decay to the SM neutrino [weighted by $(1 - |U_{\tau 4}|^2)$]. For a hypothetical mixing with the τ lepton, the total differential decay rate would then be

$$\left.\frac{\mathrm{d}\Gamma(\tau^- \to \nu h^-)}{\mathrm{d}m_h \mathrm{d}E_h}\right|_{\text{Total}} = |U_{\tau 4}|^2 \left.\frac{\mathrm{d}\Gamma(\tau^- \to \nu h^-)}{\mathrm{d}m_h \mathrm{d}E_h}\right|_{\text{HNL}} + (1 - |U_{\tau 4}|^2) \left.\frac{\mathrm{d}\Gamma(\tau^- \to \nu h^-)}{\mathrm{d}m_h \mathrm{d}E_h}\right|_{\text{SM}}. \tag{4}$$

In this analysis we search for a HNL signal by comparing the observed event yield density in the (m_h, E_h) plane to a set of template 2D histogram distributions for the backgrounds, obtained by simulating all τ known decays as well as non-τ background events, and the potential HNL signal

for different m_4 mass values. Although the invariant mass and outgoing hadronic energy (m_h and E_h) are correlated, more information can be extracted by considering both variables simultaneously.

At the *BABAR* collision energy of $\sqrt{s} = 10.58$ GeV, the process of $e^+e^- \to \tau^+\tau^-$ produces τ leptons that have decays well-separated in the c.m. frame. Candidate signal events are required to have a "1–3 topology," meaning one τ decay yields three charged particles (3-prong), while the other τ decay yields one charged particle (1-prong). Selection of the 1–3 prong decays begins by requiring events to have four well-reconstructed charged particles, none of which must be compatible with coming from a photon conversion track pair. The total charge of the four tracks must be zero. Due to the large c.m. energy relative to the τ masses, the decay daughters of the two τs tend to be well-separated. Thus, the event is divided into two hemispheres in the c.m. frame by a plane perpendicular to the thrust axis, calculated using all observed charged and neutral particles in the event. One hemisphere is required to contain just one track and is termed the "tag side." The other hemisphere (the "signal side") must include three charged tracks. All charged tracks are reconstructed assuming the pion mass hypothesis. In this analysis the 1-prong track must be identified as either leptonic channel, $\tau^- \to e^-\bar{\nu}_e\nu_\tau$ or $\tau^- \to \mu^-\bar{\nu}_\mu\nu_\tau$. These two channels have a total branching fraction of ∼35% and are chosen since they result in a better suppression of low-multiplicity $q\bar{q}$ background events. The terms "electron tag" and "muon tag" refer to the leptons produced within the 1-prong channel. Each 1-prong channel is analyzed separately. The electrons are selected using a likelihood method and the muons are found using a set of selection criteria which employ information from all five subdetectors.

V. SIMULATION

A. Background samples

There are three source of potential backgrounds:

(1) $\tau^- \to \pi^-\pi^-\pi^+\nu_\tau$, with an outgoing SM neutrino;
(2) other SM τ decays that have been misidentified as the 3-prong (3 charged pion) decay; and
(3) non-τ backgrounds that have been misidentified as the 3-prong decay.

In this analysis the SM background yields are estimated from Monte Carlo (MC) simulations, which are then passed through the same reconstruction and digitization routines as the data. The following sections describe the origins of each type of background and outline how MC simulations were generated.

1. τ backgrounds

All τ-pair events within *BABAR* are simulated with higher-order radiative corrections using the KK2F MC generator [38]. The τ-lepton decays are simulated using TAUOLA [39], which uses the averaged experimentally measured τ branching rates as listed in Ref. [3].

Additional τ backgrounds originate when τ-lepton decay modes other than the $\tau^- \to \pi^+\pi^-\pi^-\nu_\tau$ decay are misidentified as that channel. The largest contributions will come from channels with additional neutral particles; $\tau^- \to \pi^+\pi^-\pi^-\nu_\tau + N\pi^0$, where $N = 1, 2, 3\ldots$. The $N = 1$ channel will provide the largest contribution. A small amount of background events originate from kaon channels such as $\tau^- \to K^+K^-K^-\nu_\tau$, $\tau^- \to 2K^\pm\pi^\pm\nu_\tau$ and $\tau^- \to K^-\pi^-\pi^+\nu_\tau$, where one or more charged kaons are tagged as pions.

2. Non-τ backgrounds

Several non-τ backgrounds are also possible, including:

(i) $e^+e^- \to \Upsilon(4S) \to B^+B^-$ and $e^+e^- \to \Upsilon(4S) \to B^0\bar{B}^0$, which are simulated using EvtGen [40];
(ii) $e^+e^- \to u\bar{u}, d\bar{d}, s\bar{s}$ and $e^+e^- \to c\bar{c}$, which are simulated using JetSet [41,42]; and
(iii) $e^+e^- \to \mu^+\mu^-(\gamma)$, which are simulated using KK2F [43].

Bhabha events, $e^+e^- \to e^-e^+(\gamma)$, are not a source of significant background after the event selection described below is applied. Any contamination from Bhabha events will be quantified and included as a systematic in the final analysis.

B. Signal samples

A total of 26 signal samples were simulated, one for each of the HNL masses across the range 100 MeV/$c^2 < m_4 <$ 1300 MeV/c^2, at 100 MeV/c^2 increments. For each of these HNL masses both a τ^+ and τ^- signal channel were simulated. We assume a HNL could appear in either channel.

Signal samples were produced within the *BABAR* software environment using KK2F and TAUOLA by changing the value of the outgoing neutrino mass in TAUOLA. The generated signal was then passed through the same digitization and reconstruction model as the SM background and data samples.

Figure 1 shows a few 1D projections of the reconstructed invariant-mass (m_h) and c.m. energy (E_h) of the outgoing hadronic system, as fractions of that of the τ lepton, for various HNL mass hypotheses. The signal samples all have 2×10^6 reconstructed events to allow direct comparisons of the differences in shape. The reason for acquiring such high statistics is to help reduce statistical fluctuations and to ensure that tail regions are well populated. As the HNL mass increases the fraction of the tau's energy and mass going to the visible, hadronic, system decreases. The same effect is visible in Fig. 2 which shows examples of the 2D reconstructed templates.

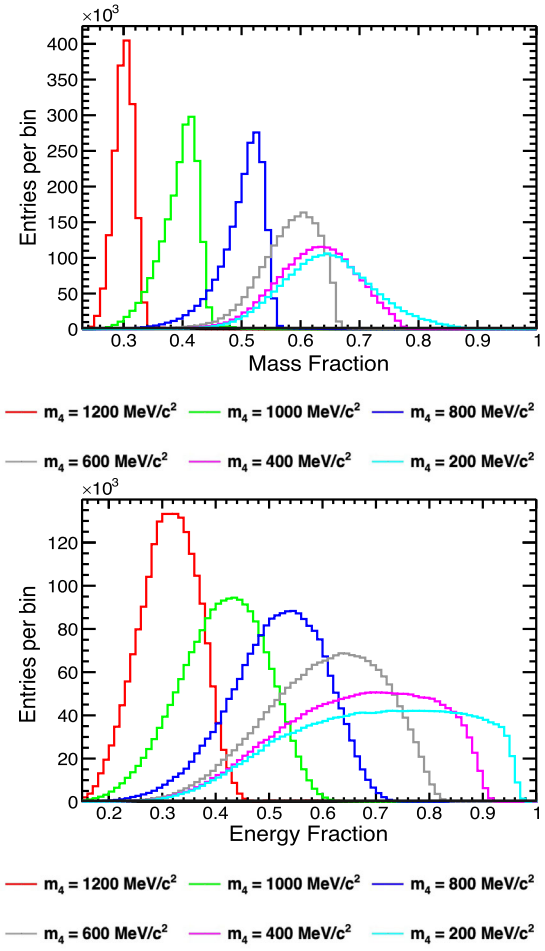

FIG. 1. 1D projections of the (top) reconstructed invariant-mass and (bottom) reconstructed energy of the outgoing hadronic system from $\tau^- \to \pi^-\pi^-\pi^+ + \nu_4$, as fractions of that of the τ-lepton, for some of the HNL mass hypotheses studied. Samples are normalized for a nominal 2×10^6 reconstructed signal events to allow direct comparisons between the samples.

C. Digitization modeling, triggering, and reconstruction

The propagation of particles through the detector geometries is simulated using the GEANT4 toolkit [44]. *BABAR*-specific software is then used to convert the GEANT4 outcome into simulated digitized raw data, which was then subjected to full reconstruction. In this analysis simulated events for HNL signal and SM processes are reconstructed in the same manner as the data. The simulation takes into account the variation of the detector and trigger configurations as well as the accelerator conditions and the beam-induced background. Trigger and filter algorithms corresponding to those applied to the real data are applied to all the simulated data. Real-data selected events, corresponding to noncolliding-beam backgrounds from the accelerator, are mixed with simulated events.

VI. EVENT SELECTION

Section IV details the initial event selection and how the topology of the events are selected. In addition, backgrounds from $q\bar{q}$ and two-photon events have a more spherically symmetric shape and lower thrust than the events from τ-pairs. Therefore, a thrust higher than 0.85 is required. This reduces contamination from $e^+e^- \to q\bar{q}$ backgrounds to ∼0.1% of the 3-prong candidates. This thrust requirement removes only ∼4% of all τ events. To reject events that do not have missing particles the p_T is required to be greater than 0.9% of the c.m. energy. A requirement on the missing momentum in the c.m. frame of $>0.9\%\sqrt{s}$ is enforced to suppress the remaining non-τ background events, including those from two-photon processes. In order to ensure a good particle identification (PID) performance, each track is required to be within the geometrical acceptance of the DIRC and the EMC: $-0.76 < \cos(\theta) < 0.9$. In addition, the track must have a minimum p_T of 250 MeV/c, enabling them to reach the DIRC. The invariant-mass of the 3-prong system, m_{123}, must be less than or equal to the τ-lepton mass (1.776 GeV/c^2).

Any event containing a track compatible with being a daughter of a converted photon [45] is rejected if $m_\gamma <$ 15 MeV/c^2, where m_γ is the converted photon candidate mass, and $\delta_{xy} < 0.5$ cm, $\delta_z < 1.0$ cm, and $r_{xy}/\sigma_{r_{xy}} > 2.5$; where δ_{xy} and δ_z are the distances of closest approach of the charged tracks from the conversion in the transverse and longitudinal directions, respectively, and $r_{xy}/\sigma_{r_{xy}}$ is the ratio of the fitted vertex decay length to the error on that value.

Events containing a K_S^0 are considered to be backgrounds. Candidate K_S^0 events are identified as a pair of oppositely charged particles in the signal hemisphere with a dipion invariant-mass consistent with K_S^0 mass, and with a decay length in the xy-plane greater than six standard deviations. These candidates are rejected. In order to reduce backgrounds from events containing neutral particles we apply specific selection criteria to discriminate against reconstructed energy deposits in the EMC not associated with a charged track. For the leptonic, 1-prong side neutral clusters are associated with the track if:

(i) *For electrons* the neutral cluster has $E_{\rm EMC}^{\rm neut,1\text{-}prong} < 1 - 0.016\,\frac{\rm GeV}{\rm cm}\,d$ where $d < 50$ cm or, if $d > 50$ cm, $E_{\rm EMC}^{\rm neut} < 0.2$ GeV, and

(ii) *For muons* the neutral cluster has $E_{\rm EMC}^{\rm neut,1\text{-}prong} <$ 0.2 GeV,

where $E_{\rm EMC}^{\rm neut,1\text{-}prong}$ is the measured EMC energy of the extra cluster and d is the distance between the EMC cluster associated to the track and the nearest neutral cluster. The remaining neutral particles are considered to be unassociated with the cluster and the event is vetoed if:

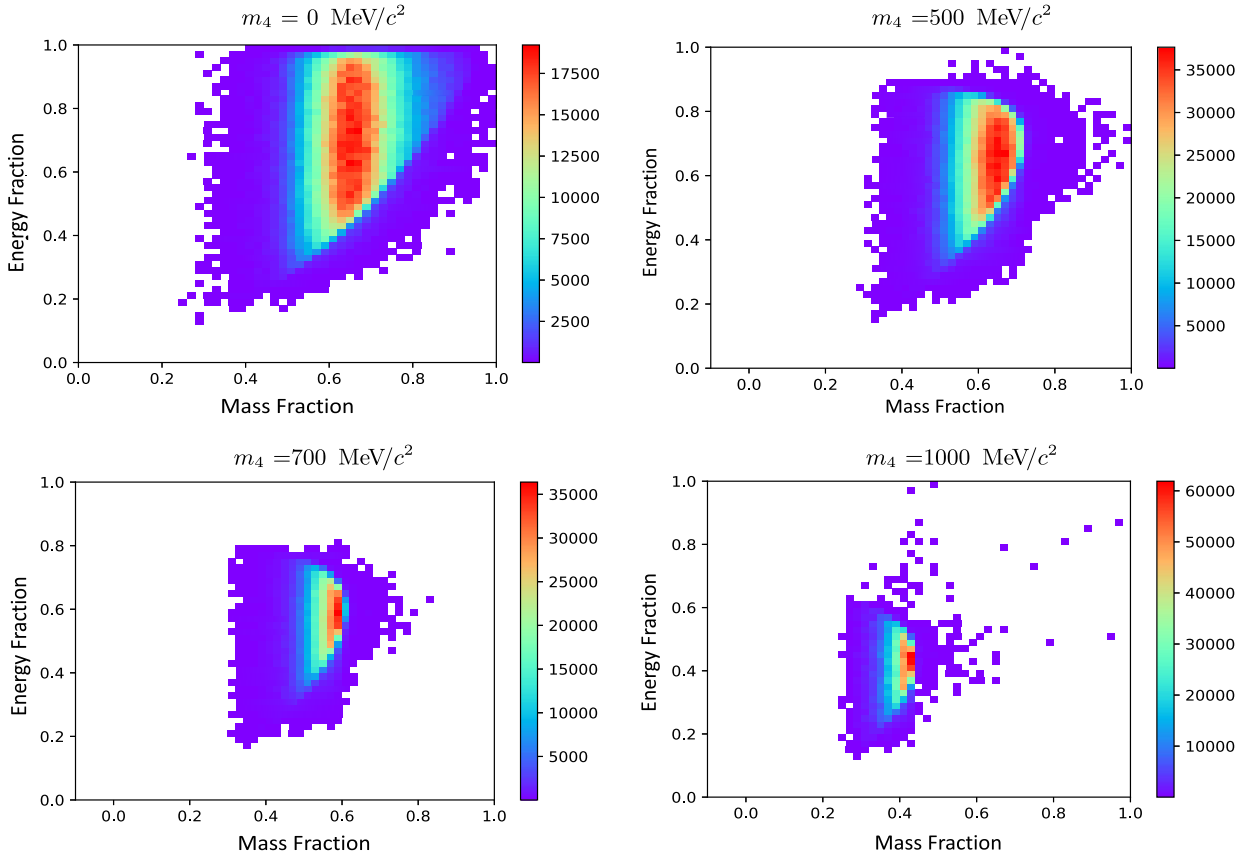

FIG. 2. Example of reconstructed invariant-mass and energy (m_h, E_h) (as fraction of incoming τ mass and energy) of the outgoing hadronic system from $\tau^- \to \pi^-\pi^-\pi^+ + \nu_4$ for HNL masses of 100, 500, 700, and 1000 MeV/c^2. No selection criteria are applied other than particle identification. The simulated signal samples in these plots assume a nonsignal (tag) τ lepton decaying leptonically to an electron and SM neutrinos.

(i) *For electrons* in the 1-prong case there is an un-associated neutral cluster with $E_{\rm EMC}^{\rm neut,1\text{-}prong} > 1$ GeV or if the 3-prong side has $\sum E_{\rm EMC}^{\rm neut,3\text{-}prong} > 0.2$ GeV.

(ii) *For muons* in the 1-prong side there is an un-associated neutral cluster with $E_{\rm EMC}^{\rm neut,1\text{-}prong} > 0.5$ GeV or if the 3-prong side has $\sum E_{\rm EMC}^{\rm neut,3\text{-}prong} > 0.2$ GeV.

VII. EXPECTED YIELD

Tables I and II list the non-negligible background yields, calculated using reconstructed MC samples (as described in Sec. V), with all selection requirements applied. By far the largest source of background comes from the SM 3-prong τ decay, that provides ∼70% of the total events. The 3-prong SM hadronic decay, accompanied by 1 or 2 neutral pions provides ∼27% of the events, the second largest contribution. The channel with two charged pions and a charged kaon, where the kaon is tagged as a pion, makes up the fourth highest contribution of the τ backgrounds. Yields from $B^0\bar{B}^0$, B^+B^- and $\mu^-\mu^+$ are expected to be very low, with the latter being completely negligible in the electron channel. The $q\bar{q}$ backgrounds make up a total ∼1–2% of the overall expected background yield.

The MC simulation yields exceed those from data by 0.48% to 0.99%.

A. Energy and mass distributions

Figures 3 and 4 show the reconstructed invariant-mass and energy fraction distributions of the hadronic system for events with an electron and muon 1-prong tag, respectively. The background uncertainty corresponds to the total uncertainty ($\pm 1\sigma_{\rm total}$) on each bin, which includes statistical uncertainty, uncertainty on τ branching fractions and uncertainties on the modeling of the underlying resonances. To account for the latter, the τ background MC distributions are reweighted to reflect an underlying resonance mass and width values at either $\pm 1\sigma$, where σ is the averaged experimental uncertainty. This will be discussed in detail in Secs. IX B 2 and IX B 3. The results of this analysis will quote two sets of limits, one which does not take into account these modeling uncertainties (and uses the average values presented in Ref. [3]), and a more conservative limit, which takes into account the largest possible deviation in

TABLE I. List of expected background yields after all selection requirements are applied for positive 3-prong channel. All backgrounds are scaled to represent what would be expected for $\mathcal{L} = 424$ fb^{-1}.

	Electron tag		Muon tag	
Background type	MC yield	[%]	MC yield	[%]
$\tau^+ \to \pi^+\pi^+\pi^-\bar{\nu}_\tau$	894864	70	810586	71
$\tau^+ \to \pi^+\pi^+\pi^-\pi^0\bar{\nu}_\tau$	332008	26	278830	24
$\tau^+ \to \pi^+\pi^+\pi^-2\pi^0\bar{\nu}_\tau$	34050	2.7	28841	2.5
$\tau^+ \to \pi^-\pi^+K^+\bar{\nu}_\tau$	3391	0.27	3101	0.27
$\tau^+ \to \pi^+\pi^+\pi^-3\pi^0\bar{\nu}_\tau$	1541	0.12	821	0.07
$\tau^+ \to \pi^+\pi^0\bar{\nu}_\tau$	498	0.039	207	0.017
$\tau^+ \to \pi^+2\pi^0\bar{\nu}_\tau$	252	0.02	92	0.008
$\tau^+ \to 2K^+\pi^-\bar{\nu}_\tau(\to K^+K^-\pi^+\bar{\nu}_\tau)$	207	0.016	146	0.013
$e^+e^- \to Y(4S) \to c\bar{c}$	8031	0.63	6512	0.55
$e^+e^- \to Y(4S) \to u\bar{u}, s\bar{s}, d\bar{d}$	542	0.043	13898	1.19
$e^+e^- \to Y(4S) \to B^0\bar{B}^0$	108	0.009	99	0.0084
$e^+e^- \to Y(4S) \to B^+B^-$	100	0.008	89	0.0076
$e^+e^- \to \mu^+\mu^-$	0	0	15	0.0013
Total MC	1278339	…	1143237	…
Data	1265698	…	1137521	…

the template histograms when the uncertainty on the modeling is accounted for. The effect of the change in the characteristics of the intermediate resonance is that events can shift into neighboring bins. This could provide a dependence on bin size (see Sec. IX).

The invariant-mass and energy distributions of the negative and positive signal channels, for the same lepton tag, are statistically consistent. The ratio plots included in these figures quantify the ratio of MC to data yield in each bin, along with statistical uncertainty on that ratio. When the background uncertainty is taken into account the MC and data distributions can be considered consistent in most bins. The mass and energy distributions associated with the electron tag and the muon tag are also similar in shape, which is to be expected. Slight differences appear due to differences in the PID algorithms and background content.

Figures 5–8 show the 2D template histograms for all the processes in the electron and muon tag, respectively (negative channel only, for simplicity). The second largest background source (after the SM 3 charged pion channel) comes from the channels which include 3-prong pionic

TABLE II. List of expected background yields after all selection requirements are applied for negative 3-prong channel. All backgrounds are scaled to represent what would be expected for $\mathcal{L} = 424$ fb^{-1}.

	Electron tag		Muon tag	
Background type	MC yield	[%]	MC yield	[%]
$\tau^- \to \pi^-\pi^-\pi^+\nu_\tau$	900069	70	817342	70
$\tau^- \to \pi^-\pi^-\pi^+\pi^0\nu_\tau$	334565	26	281613	25
$\tau^- \to \pi^-\pi^-\pi^+2\pi^0\nu_\tau$	34255	2.7	29287	2.5
$\tau^- \to \pi^+\pi^-K^-\nu_\tau$	3567	0.27	3228	0.27
$\tau^- \to \pi^-\pi^-\pi^+3\pi^0\nu_\tau$	1535	0.12	795	0.07
$\tau^- \to \pi^-\pi^0\nu_\tau$	476	0.039	217	0.019
$\tau^- \to \pi^-2\pi^0\nu_\tau$	240	0.02	92	0.08
$\tau^- \to 2K^-\pi^+\bar{\nu}_\tau(\to K^-K^+\pi^-\bar{\nu}_\tau)$	202	0.016	152	0.013
$e^+e^- \to Y(4S) \to c\bar{c}$	8031	0.63	6837	0.58
$e^+e^- \to Y(4S) \to u\bar{u}, s\bar{s}, d\bar{d}$	495	0.043	16602	1.42
$e^+e^- \to Y(4S) \to B^0\bar{B}^0$	126	0.009	98	0.0083
$e^+e^- \to Y(4S) \to B^+B^-$	93	0.008	103	0.0088
$e^+e^- \to \mu^+\mu^-$	0	0	10	0.0009
Total MC	1283654	…	1155920	…
Data	1273291	…	1150350	…

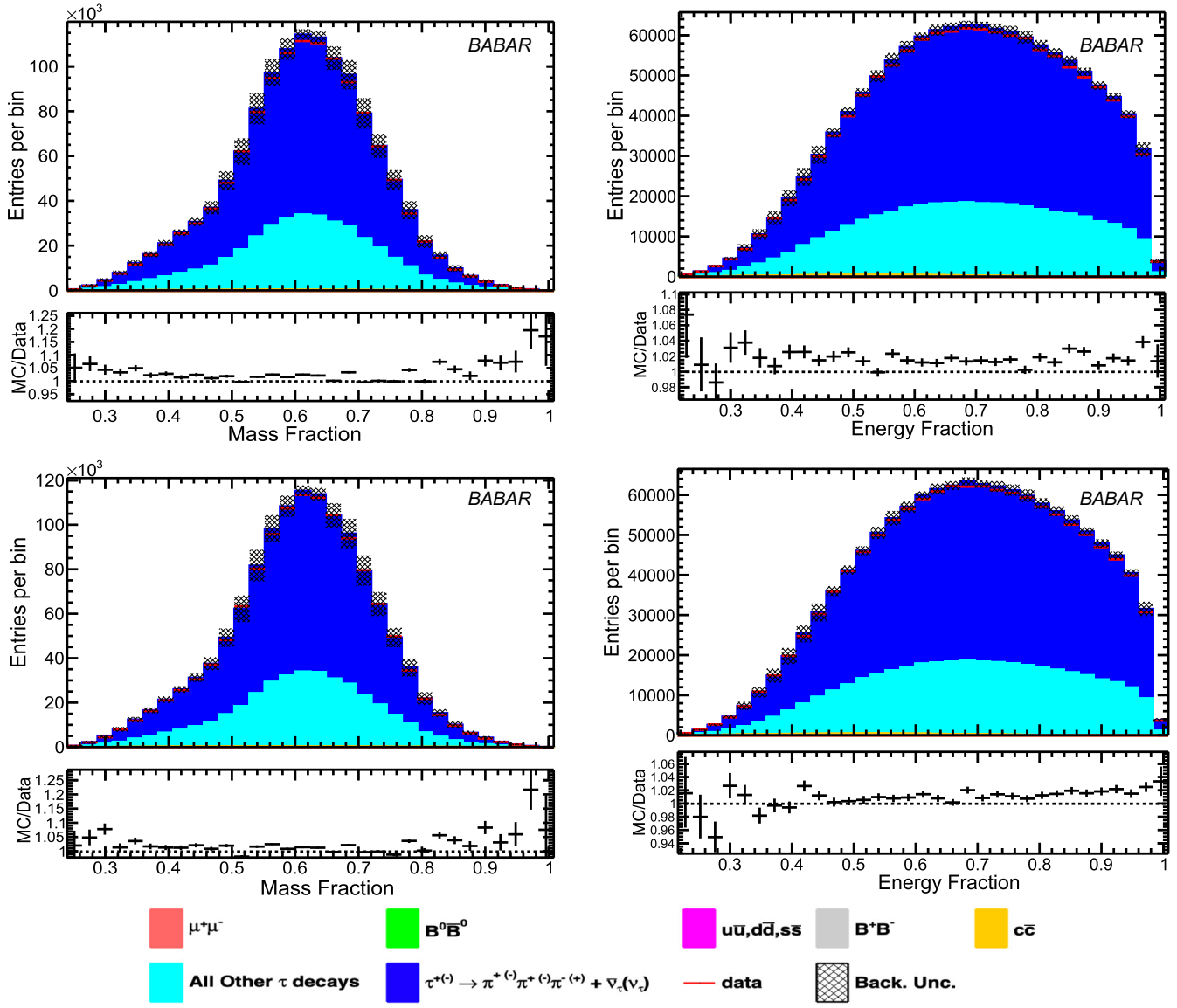

FIG. 3. *Electron tag*: Reconstructed mass (left) and energy (right) of the outgoing hadronic system, as fractions of that of the incoming τ lepton, for the (top) positive τ signal channel and (bottom) negative τ signal channel. The "All other τ" component contains all other τ decays which are not $\tau^{+(-)} \to \pi^{-(+)}\pi^{+(-)}\pi^{+(-)} + \bar{\nu}_\tau(\nu_\tau)$. The individual contributions are detailed in Tables I and II. The lower figures show ratios of the total MC yield to data yield, in each bin. The error bars are statistical.

decays, accompanied by a neutral pion, as outlined in Tables I and II. The main difference being that the mean is lowered, there is missing mass, corresponding to neutral pions. This must be well-accounted for to not misidentify this as a HNL of mass $\sim m_{\pi^0}$. Uncertainties in modeling of these nonsignal τ channels are also included in the background uncertainty shown, and will be discussed in Sec. IX B 3.

VIII. BINNED LIKELIHOOD FUNCTION

A binned likelihood approach is taken to place limits on the parameter of interest $|U_{\tau 4}|^2$, the mixing parameter between the SM τ neutrino and the HNL. It is assumed that the contents of a given bin, i, j, in the (m_h, E_h) data histogram is distributed as a Poisson distribution and may contain events emanating from any of the SM process, and potentially HNL signal events. The number of expected events reconstructed in a given bin ($\nu^{\rm reco}_{{\rm obs},ij}$) may be written as

$$\nu^{\rm reco}_{{\rm obs},ij} = (\nu_{{\rm HNL},ij} + \nu_{\tau-{\rm SM},ij} + \nu_{\tau-{\rm other},ij} + \nu_{{\rm non}-\tau,ij})^{\rm reco}, \tag{5}$$

where $\nu_{{\rm HNL},ij}$ is the expected number of signal events, $\nu_{\tau-{\rm SM},ij}$ represents the expected number of events from

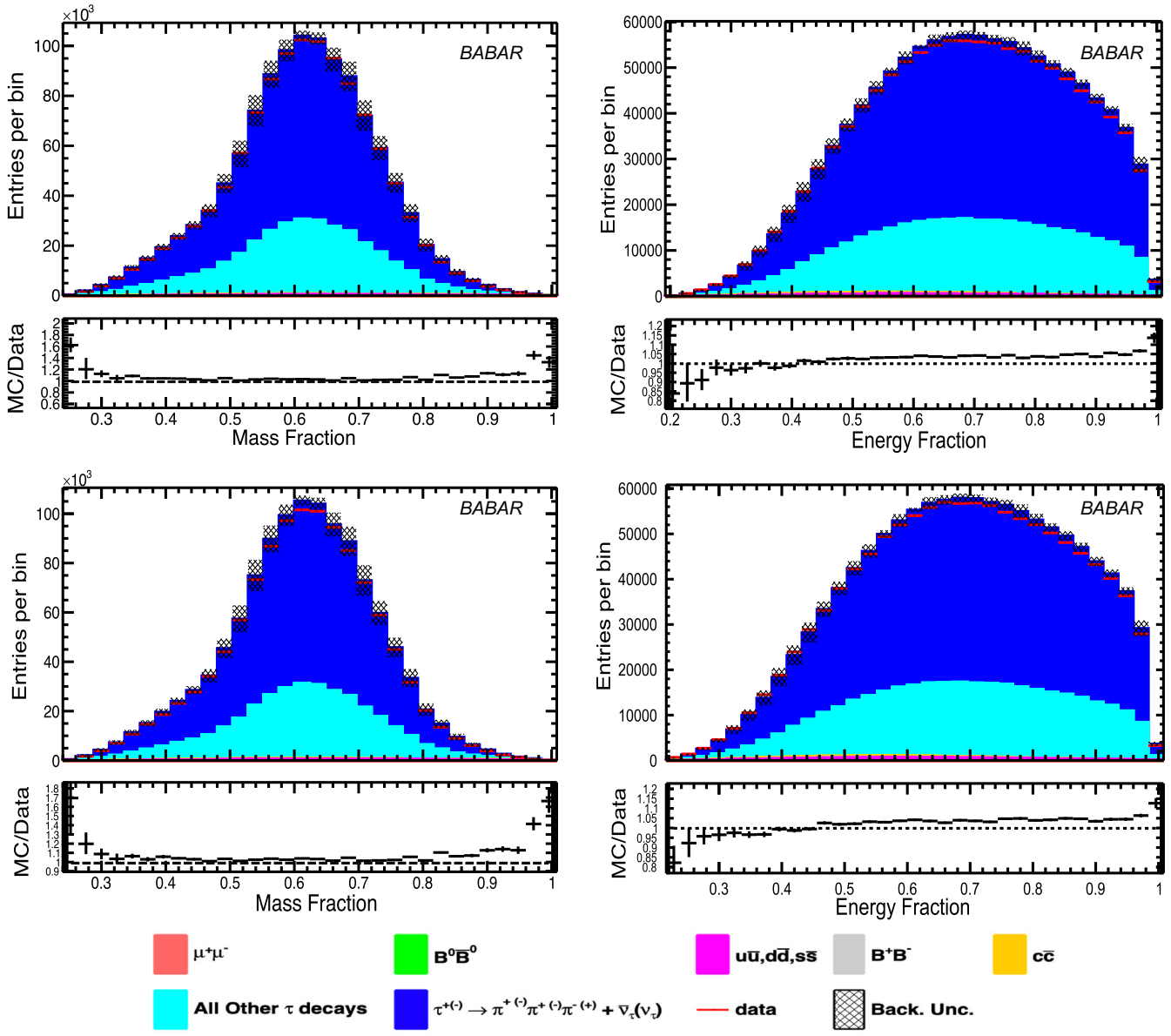

FIG. 4. *Muon tag*: Reconstructed mass (left) and energy (right) of the outgoing hadronic system, as fractions of that of the incoming τ lepton, for the (top) positive τ signal channel and (bottom) negative τ signal channel. The "All other τ" component contains all other τ decays which are not $\tau^{+(-)} \to \pi^{-(+)}\pi^{+(-)}\pi^{+(-)} + \bar{\nu}_\tau(\nu_\tau)$. The individual contributions are detailed in Tables I and II.

the SM $\tau^- \to \pi^-\pi^-\pi^+\nu_\tau$ decay, and $\nu_{\tau-\text{other},ij}$ and $\nu_{\text{non}-\tau,ij}$ are the expected SM other τ and non-τ backgrounds, respectively. The values of $\nu_{\tau-\text{SM},ij}$, $\nu_{\tau-\text{other},ij}$ and $\nu_{\text{non}-\tau,ij}$ are inferred from MC simulation; ν_{HNL} must be estimated using our 2D template histograms for a given mass.

Denoting the number of generated τ-lepton events in the sample from a specific tag as

$$N_{\tau,\text{gen}} = \mathcal{L}_{\text{int}} \cdot \sigma(ee \to \tau\tau) \cdot \text{BR}(3\text{-prong}) \cdot \text{BR}(1\text{-prong}), \tag{6}$$

the numbers of expected signal, SM τ3-prong, and other background events are written more simply as

$$\hat{\nu}_{\text{HNL},ij} = n^{\text{reco}}_{\text{HNL},ij} = N_{\tau,\text{gen}} \cdot (|U_{\tau 4}|^2) \cdot p_{\text{HNL},ij}, \tag{7}$$

$$\hat{\nu}_{\tau-\text{SM},ij} = n^{\text{reco}}_{\tau-\text{SM},ij} = N_{\tau,\text{gen}} \cdot (1 - |U_{\tau 4}|^2) \cdot p_{\tau-\text{SM},ij}, \tag{8}$$

and

$$\hat{\nu}_{\text{BKG},ij} = n^{\text{reco}}_{\text{BKG},ij} = n^{\text{reco}}_{\tau-\text{other},ij} + n^{\text{reco}}_{\text{non}-\tau,ij}, \tag{9}$$

where the final term ($\hat{\nu}_{\text{BKG},ij}$) is a combination of all the backgrounds not associated with a $\tau^- \to \pi^-\pi^-\pi^+\nu_\tau$ channel, calculated from MC. The p_{ij} terms are the products of the reconstruction efficiency ($\epsilon^{\text{reco}}_{ij}$—the probability that, given an event took place, that the reconstruction

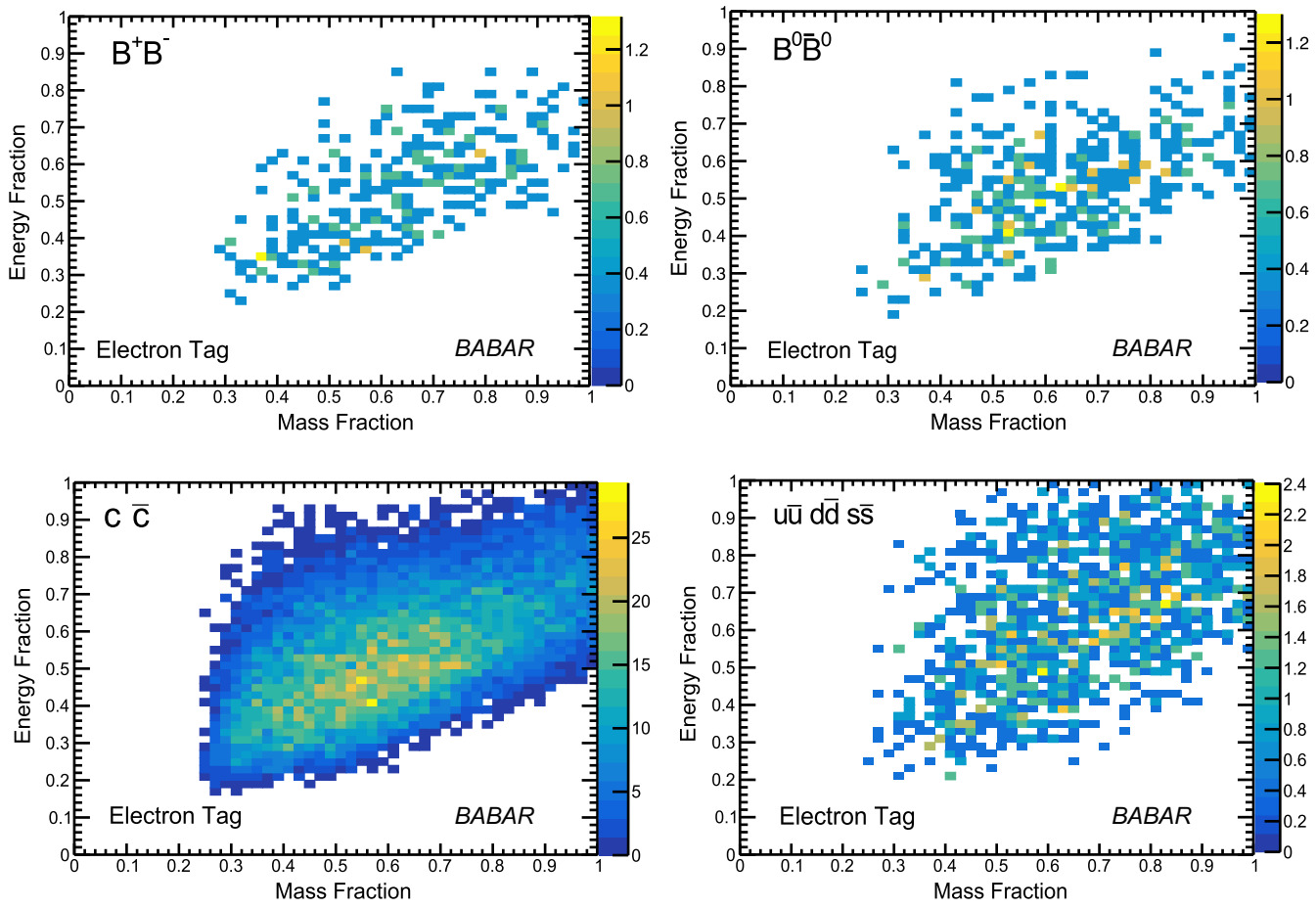

FIG. 5. *Electron tag* (non-τ): 2D templates showing reconstructed invariant mass and energy (as fraction of incoming τ mass and energy) for SM non-τ background processes, the $\mu^+\mu^-$ background is not shown since the yield is zero.

algorithms find it), selection efficiency ($\epsilon_{ij}^{\rm sel}$—the probability that the reconstructed event passes the event selection in this analysis), and $p_{ij}^{\rm shape}$ (the fraction of total histogram reconstructed and selected events present in the ijth bin) for each process.

The likelihood to observe the selected candidates in all the (m_h, E_h) bins is the product of the Poisson probability to observe the selected events in each bin,

$$\mathcal{L} = \prod_{ij} f(n_{ij}; n_{\rm obs}, \vec{\theta}) = \prod_{ij} \frac{(\nu_{\rm HNL} + \nu_{\tau-{\rm SM}} + \nu_{\rm BKG})_{ij}^{(n_{\rm obs})_{ij}} e^{-(\nu_{\rm HNL}+\nu_{\rm BKG}+\nu_{\tau-{\rm SM}})_{ij}}}{(n_{\rm obs})_{ij}!} \prod_k f(\theta_k, \tilde{\theta}_k), \tag{10}$$

where $n_{\rm obs}$ is the number of events observed in the data and $\vec{\theta}$ describes a number of nuisance parameters corresponding to the yield uncertainties outlined in Sec. IX. The final product in this expression represents the product of the nuisance parameters. Each parameter, k, will be modeled using a Gaussian probability density function; $f(\theta_k, \tilde{\theta}_k)$. Each $f(\theta_k, \tilde{\theta}_k)$ term represents the probability for the true value of a nuisance parameter to be equal to θ_k, given that the best estimate of the parameter is $\tilde{\theta}_k$, which is determined using the methods outlined in Sec. IX.

Substituting in the expressions for the estimators of the expected yields gives

$$\mathcal{L} = \prod_{\rm charge}^{+-} \left(\prod_{\rm channel}^{e\mu} \left(\prod_{\rm bin}^{ij} \left(\frac{1}{n_{{\rm obs},ij}!} \left[N_{\tau,{\rm gen}} \cdot |U_{\tau 4}|^2 \cdot p_{{\rm HNL},ij} + N_{\tau,{\rm gen}} \cdot (1 - |U_{\tau 4}|^2) \cdot p_{\tau-{\rm SM},ij} + n_{{\rm BKG},ij}^{\rm reco} \right]^{(n_{\rm obs})_{ij}} \right.\right.\right.$$
$$\left.\left.\left. \times \exp\left[-(N_{\tau,{\rm gen}} \cdot |U_{\tau 4}|^2 \cdot p_{{\rm HNL},ij} + N_{\tau,{\rm gen}} \cdot (1 - |U_{\tau 4}|^2) \cdot p_{\tau-{\rm SM},ij} + n_{{\rm BKG},ij}^{\rm reco}) \right] \right) \right)_{\rm bin} \times \prod_k f(\theta_k, \tilde{\theta}_k) \right)_{\rm channel} \Bigg)_{\rm charge}. \tag{11}$$

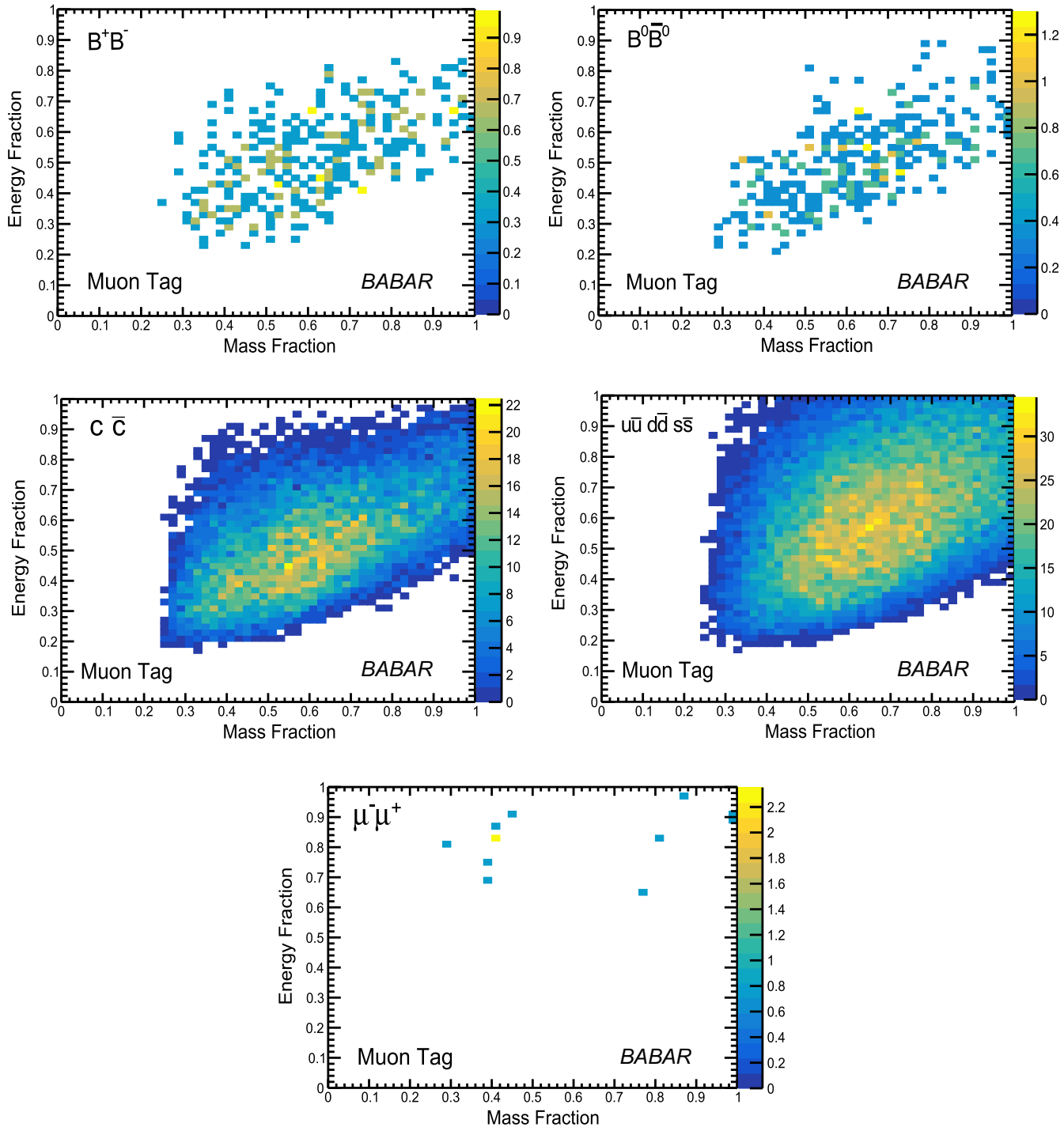

FIG. 6. *Muon tag* (non-τ): 2D templates showing reconstructed invariant mass and energy (as fraction of incoming τ mass and energy) for SM non-τ background processes.

The expression involves a product over all bins, ij, over the two 1-prong channels, and over both possible τ-lepton charges ($\pm$).

In this analysis it is assumed that the *BABAR* modeling and reconstruction software offers a realistic representation of the physics processes, the experimental environment and the response of the detectors to the data. Any known cause of a discrepancy between the data and MC must be characterized as an uncertainty.

Reference [46] gives an overview of the process of incorporating nuisance parameters into a binned Poisson likelihood such as that presented. The expected number

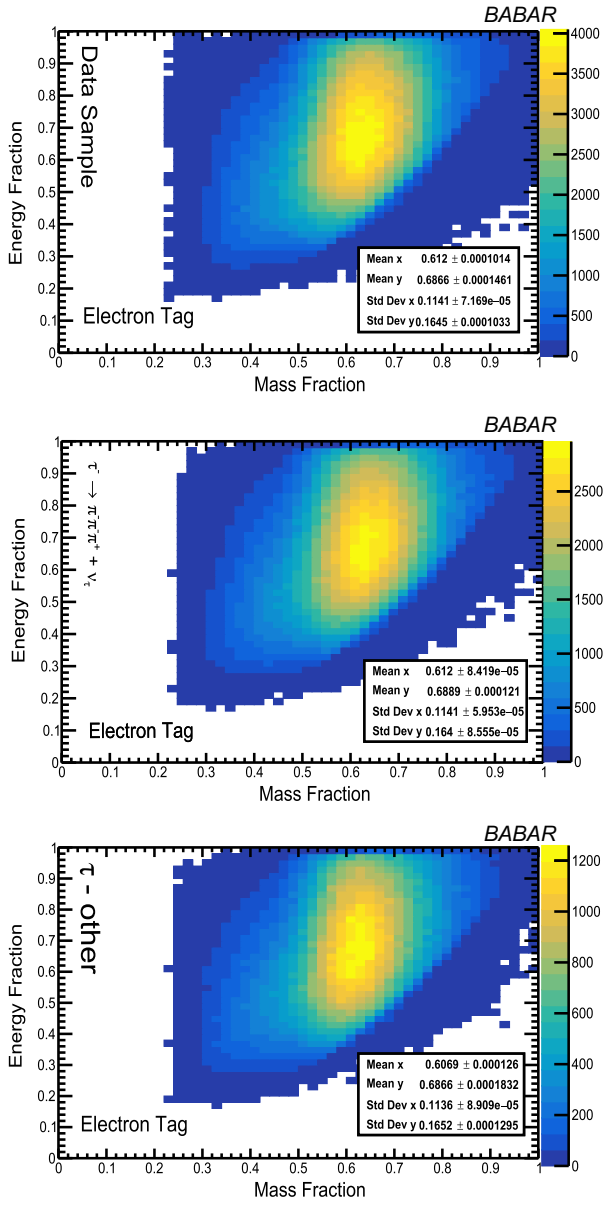

FIG. 7. *Electron tag*: 2D Templates of reconstructed hadronic invariant mass and energy (m_h, E_h) (as fraction of incoming τ mass and energy) for data (top), SM τ MC template for $\tau^- \to \pi^-\pi^-\pi^+\nu_\tau$ (middle) and all other τ decays (bottom).

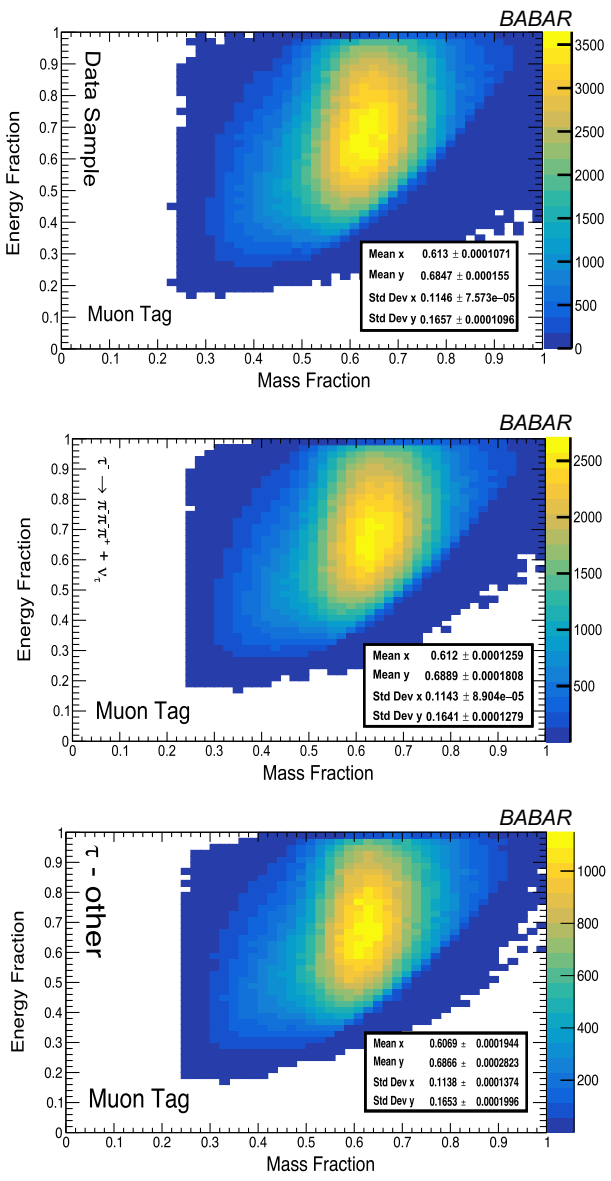

FIG. 8. *Muon tag*: 2D Templates of reconstructed hadronic invariant mass and energy (m_h, E_h) (as fraction of incoming τ mass and energy) for data (top), SM τ MC template for $\tau^- \to \pi^-\pi^-\pi^+\nu_\tau$ (middle) and all other τ decays (bottom).

of signal and background events are functions of a set of nuisance parameters ($\vec{\theta}$). These represent the systematic yield uncertainties to be outlined in Sec. IX. Incorporation of shape uncertainties is described in Secs. IX B 2 and IX B 3.

Two hypotheses can be proposed regarding the content of the data:

(i) H_0: where the signal is present at some level, $|U_{\tau 4}|^2_0$.
(ii) H_1: where the data is a mixture of background + signal, with small signal present.

A likelihood ratio test statistic (LR) is used to test hypothesis H_0 against H_1,

$$LR = \frac{\mathcal{L}_{H_0}(|U_{\tau 4}|^2_0; \hat{\hat{\theta}}_0, \text{data})}{\mathcal{L}_{H_1}(|\hat{U}_{\tau 4}|^2; \hat{\theta}, \text{data})}, \tag{12}$$

where $\mathcal{L}$ in both numerator and denominator describes the maximized likelihood, for two instances. The denominator is the maximized (unconditional) likelihood giving the maximum likelihood estimator of $|U_{\tau 4}|^2$ and the set of nuisance parameters ($\hat{\theta}$); $\hat{\theta}$ is a vector of nuisance parameters which maximize the likelihood. In the numerator the nuisance parameters are maximized for a given value of $|U_{\tau 4}|^2$ i.e. it is the conditional maximum-likelihood. The ratio, LR, is consequently a function of $|U_{\tau 4}|^2$ through the

numerator. It must be noted that the numerator denotes the hypothesis for any given value of $|U_{\tau 4}|^2$ (including the background only case i.e. $|U_{\tau 4}|^2 = 0$). Reference [47] provides more details on likelihood-based tests.

A test statistic, q, can be defined as

$$q = -2\ln\left(\frac{\mathcal{L}_{H_0}(|U_{\tau 4}|_0^2; \hat{\hat{\theta}}_0, \text{data})}{\mathcal{L}_{H_1}(|\hat{U}_{\tau 4}|^2; \hat{\theta}, \text{data})}\right) = -2\ln(\Delta\mathcal{L}). \quad (13)$$

Using Wilk's theorem [48], q asymptotically approaches a χ^2 distribution under H_0. To find a $100(1-\alpha)\%$ confidence interval we move to the left and to the right of the minimum value of q to find the points where the function increases by the α percentile of a χ^2 distribution with a number degrees of freedom equal to the number of parameters.

IX. SYSTEMATIC UNCERTAINTIES

There are two types of systematic uncertainty which must be accounted for:

(1) *Normalization uncertainties* which affect the overall expected yield of a particular background or signal events. These uncertainties affect all bins uniformly.
(2) *Shape uncertainties* which affect the shape of either the background or signal in the template histograms (in the (m_h, E_h) plane). These affect the signal/background yield in a specific bins differently and may mean that template distribution shapes are shifted nonuniformly.

Since the expected background contributions are estimated using MC simulations, any uncertainty on that MC can affect how accurately it represents the real data. Therefore, in the following discussion emphasis is placed on quantifying sources of deviation between the MC and data and the impact of these uncertainties on the final result.

A. Normalization uncertainties

Normalization uncertainties are incorporated into this analysis as nuisance parameters, parametrized as Gaussian functions, unless otherwise stated.

1. Luminosity

Uncertainty on the luminosity are calculated from experimental systematic uncertainties on the Bhabha and muon-pair selections used in luminosity determination. The uncertainty is run-dependent and averages at 0.44% [35].

2. Cross section

There is an uncertainty associated with the τ-pair production cross section $\sigma(e^+e^- \to \tau^+\tau^-) = 0.919 \pm 0.003$ nb. A relative uncertainty of 0.3% is assigned.

3. Uncertainties in τ decay-mode branching fractions

The decay branching fractions for the τ-lepton decay modes used within TAUOLA were updated to reflect the current best-fit values listed in Ref. [3]. Each of these is an average from several experimental results and each has an associated error.

This uncertainty will affect the yield of each τ related channel across all bins i.e. it is a scaling factor. It should not affect the shape of the template histograms. To account for these uncertainties the yields of each of these backgrounds are varied by $\pm 1\sigma$ on the listed percentage and the final analysis is repeated. The overall variation is included in the systematic uncertainty on the final result. The systematic uncertainty on the final result, due to these branching fraction uncertainties is very small $\ll 0.1\%$.

4. PID efficiencies

In this analysis we rely on the *BABAR* PID algorithms [35] to accurately select leptonic 1-prong and hadronic 3-prong events in both the MC and data samples.

The electron selection algorithm has an efficiency of above 90% and a pion misidentification rate between 0.05%–0.01%. Efficiencies for negative and positive tracks were equivalent. We estimate a systematic uncertainty of 2% to be consistent with the observed variations of data and MC.

This muon selection algorithm has an efficiency of ∼80% and a mis-identification rate of >1.5%. Only small differences between MC and data was observed in the test sample, therefore, a systematic uncertainty of 1% is assigned.

For the 3-prong hadronic channel the pion selection algorithm has an efficiency of above ∼85%, a kaon mis-identification rate of ∼2–4%, an electron mis-identification rate of ∼5%, and a muon mis-identification rate of ∼20%. A systematic uncertainty of 3% is assigned.

All PID uncertainties are included as nuisance parameters.

5. Bin size

Altering the number of bins in the 2D template histograms by double or half the number of bins had a small effect of 0.2% on the end result.

6. Other systematic uncertainties

The following systematic uncertainties were ignored in the final study:

(1) *Tracking efficiency*
The tracking efficiency has been measured in a general purpose *BABAR* collaboration study using control samples of charged tracks for both MC and data for all run periods. The total uncertainty (average for all runs) is 0.5%. Since the simulation

and data samples efficiency are consistent, within uncertainties, no efficiency correction is applied.

(2) *Trigger and filter efficiency*
Corrections to account for differences in the filter and trigger efficiency are found to be negligible.

(3) *Modeling of detector response*
Deviations between data and MC due to detector response modeling are negligible.

(4) *Beam energy*
There is a systematic uncertainty associated with the uncertainty on the beam collision energy. The systematic resulting from the c.m. energy scale and energy spread was determined as the maximum shift resulting from varying the c.m. energy in the MC by ± 2 MeV. This was found to have negligible effect on the final result.

(5) *Tau mass*
The uncertainty on the τ mass ($m_\tau = 1776.99 \pm 0.29$ MeV$/c^2$) [3] has insignificant effect on the results.

(6) *τ polarization*
No systematic effect is expected from τ polarization.

B. Shape uncertainties

Uncertainties on signal and background shapes require more careful analysis. These include:

1. Uncertainties on non-τ backgrounds

(i) The side band region above the 3-prong invariant-mass requirement, $m_{123} > 1.77$ GeV$/c^2$ is used to determine the deviation between data and the $q\bar{q}$ background distributions. The data were found to disagree with the MC in this region by $<0.1\%$.

(ii) The generic τ-lepton MC does not contain Bhabha backgrounds. In this analysis all of the hadronic (3-prong) tracks were required to fail the electron PID selector. To estimate Bhabha contamination, this requirement was loosened to require only 0, 1 or 2 pions to fail the electron PID and then measuring the percent deviation between the data and MC in the region $0.6 < 2p_{c.m.} \cdot c < 0.9$, the control region for the Bhabha background, where $p_{c.m.}$ is the momentum in the c.m. frame. Using the percentage changes as each requirement is removed one can extrapolate the expected percentage difference between MC and data for the case when the requirement is enforced for all 3 pions in the 3-prong side. The estimated contamination in the control region is 0.2%.

Using these methods a total 0.3% uncertainty is assigned for these two non-τ backgrounds. This is included in the background uncertainty.

2. Uncertainty on modeling of a_1 resonance

For many hadronic τ decay channels the relative uncertainties from experimental results are large, and their modeling in TAUOLA is discussed in detail in Ref. [39].

A τ-lepton decay to an odd number of pions occurs almost exclusively through the axial-vector current, and the 3-prong pionic τ-lepton decay is mediated by a $a_1(1260)$ meson with quantum numbers $J^{PC} = 1^{++}$ in 97% of cases. The $a_1(1260)$ resonance decays through the intermediate $\rho\pi$ state.

The experimental data on the $a_1(1260)$ may be grouped into two classes: hadronic production and τ-lepton decays. In the MC samples used in this analysis the PDG [3] average of $m_{a_1} = 1230 \pm 40$ MeV$/c^2$ and Breit-Wigner averaged width of $\Gamma_{a_1} = 420 \pm 35$ are used. These averages include many different experiments, which look at both types of data. The uncertainty associated with the a_1 resonance represents the dominant contribution to the systematic error in our measurement.

In order to understand the effects of the uncertainty on the a_1 mass on the final results in this analysis several additional MC simulations were built. This included two sets of samples for each HNL mass hypothesis (and the SM scenario), where the m_{a_1} was varied to $\pm 1\sigma$ of the experimental average (where $\sigma = 40$ MeV$/c^2$). The simulation source code was altered to use these masses instead of the average, and the τ decays were resimulated in the same way so described in Sec. V B. For each $\pm 1\sigma$ value, sufficient statistics were generated to ensure $\sim\mathcal{O}(10^6)$ events were reconstructed. These were then used in the final analysis to reweight the 2D template for signal sample and entire τ MC sample. An event-by-event reweighting was applied to the reconstructed samples and the same selection requirements were applied. The reweighted samples were run through the same analysis code as the full unweighted data set and the limit on $|U_{\tau 4}|^2$ recalculated for each $\pm 1\sigma$ mass value. The largest variation in the result will be quoted as a systematic uncertainty in Sec. X.

Figure 9 shows the example reconstructed 2D template histograms for several HNL mass hypotheses. Section ?? lists the relative shift in the means and variances of the distributions for each altered template. These relative shifts get smaller as the neutrino mass increases. For the 0 MeV$/c^2$ scenario the mean shifts by around $\pm 2.1\%$ in m_h/m_τ and around $\pm 1.2\%$ in E_h/E_τ. For the case with $m_4 = 500$ MeV$/c^2$ the mean shifted by around $\pm 1.2\%$ in m_h/m_τ and around $\pm 0.5\%$ in E_h/E_τ. At $m_4 = 1000$ MeV$/c^2$ the shift in E_h/E_τ disappears and the shift in m_h/m_τ is just $\pm 0.8\%$. This is due to the allowed phase space of the hadronic system being substantially diminished as the mass of the invisible component increases. The heavier HNL takes a much larger fraction of the available energy and, therefore, the shift in the visible distributions becomes less apparent.

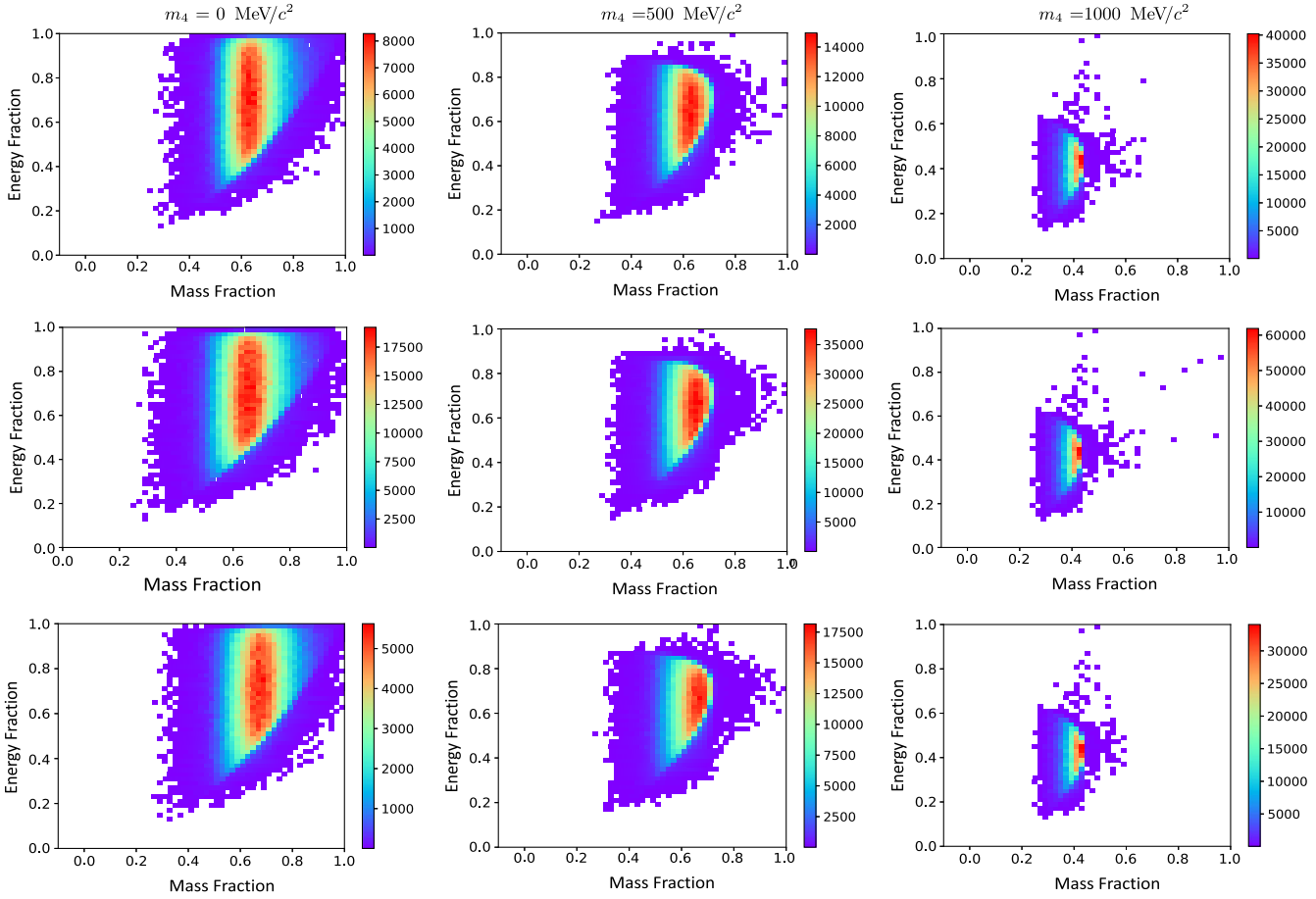

FIG. 9. Examples of reconstructed outgoing hadronic invariant mass and energy (m_h, E_h) (as fraction of incoming τ mass and energy) for HNL masses of $m_4 = 0$ MeV/c^2 (left column), 500 MeV/c^2 (middle column), and 1000 MeV/c^2 (right column) for three m_{a_1} possibilities: 1190 MeV/c^2 (top row), 1230 MeV/c^2 (middle row), and 1270 MeV/c^2 (bottom row). These samples are used to reweight the 2D template histograms and the shift in the derived value of $|U_{\tau 4}|^2$ is quoted as an uncertainty.

A shift in reconstructed mass and energy within a bin has no effect on the end result. However, if the difference in the template is large enough it can result in events being shifted by a bin (or possibly more) relative to the distribution when the average quantities are used. Each axis has 50 bins. For the mass axis each bin represents $m_\tau/50 \simeq 35$ MeV/c^2, for the energy axis, the fraction depends on the incoming τ c.m. energy which has a maximum around $\sqrt{s}/2$ GeV, meaning a bin width of ~100 MeV. Of course, depending where the event lies within the bin, shifts in less than these values can still result in it moving bins. When the mass is shifted to the lower value the mean of the distribution in both m_h and E_h becomes lower, since the incoming mass energy is lower, when the higher m_{a_1} is used the opposite is true. The effects are symmetric about the average, $m_{a_1} = 1230$ MeV/c^2, case.

To understand the effect of the experimental uncertainty on the value of Γ_{a_1} on the end result, again additional samples were made using widths at either experimental average $\pm 1\sigma$ value, where $\sigma = 35$ MeV/c^2. The resulting shifts in the mean and rms values of the 2D templates are relatively small ($\ll$1% for the both SM and signal cases). In the case of the signal samples, the relative effect gets smaller with increased outgoing HNL mass and becomes negligible for HNL masses >1000 MeV/c^2, in all instances the effect is small.

It must be recognized, however, that the experimental values presented in Ref. [3] span a wide range. The PDG estimates that the width is in fact somewhere between 250–600 MeV/c^2. This is a conservative band and the averaged value is contained within this estimated band. To assess the effect of this conservative uncertainty, the width was again shifted to these two values. This results in a relatively large shift of up to ~6–7% in the m_h/m_τ rms values, with the E_h/E_τ shifting by ~1–3%. For both axes the mean values shift by only ~1–2% for the SM scenario. The heavier HNL signal samples are again less effected by the change.

In the final result the uncertainty on the width values will be taken from the largest change in the final result when the more conservative, estimated, widths are considered.

3. Uncertainties in modeling of other τ channels

There are two other dominant τ channels in this analysis, $\tau \to 3\pi^{\pm} + \pi^0$ and $\tau \to 3\pi^{\pm} + 2\pi^0$, with the former being, by far, the largest. These other hadronic τ-decay channels involve several other intermediate states; TAUOLA models these multipion channels in an oversimplified way. The spectral functions involved are calculated using data. To understand the impact of uncertainty from the modeling of these modes the reconstructed samples can be reweighted to reflect the reconstructed mass/energy obtained when the masses used for the intermediate mesons in these decay models are varied to the PDG $\pm 1\sigma$ values. This follows the same technique as described in the previous section.

Uncertainties in all τ hadronic models are included in the background uncertainty displayed in Figs. 3 and 4. The impact of these uncertainties in the 3-prong and other τ background shapes will be quoted in the final result as the "modeling uncertainty."

C. Systematic uncertainty summary table

Table III lists the relative contribution for each of the systematic uncertainties discussed in this section.

X. RESULTS

For the final results, and following Eq. (11), the data from the two channels were combined, assuming *CPT* symmetry holds, and the coupling to neutrinos and antineutrinos is identical. Figure 10 shows the upper limit at the 95% confidence level provided by this analysis using the binned likelihood technique described in Sec. VIII. The magenta line represents the upper limit when all systematic uncertainties are considered. To characterize deviations due to the uncertainty on Γ_{a_1} the more conservative PDG estimates are used. The dominant systematic uncertainty is, by far, that due to the assumptions made within our hadronic modeling, the main contribution being uncertainty in the intermediate resonances for the τ 3-prong channel, and the dominant τ backgrounds. Table IV lists these 95% CL upper limits derived for each HNL mass hypothesis, with and without the systematic uncertainties considered. The "with systematic uncertainty" is a conservative calculation, which includes the largest discrepancies possible in the 2D fits with consideration of experimental limits on the resonances. The relative systematic uncertainty decreases as the mass of the hypothetical HNL increases, which is expected since it was shown in

TABLE III. Systematic uncertainty contribution to the event yield (in %) from each source, based on comparisons between MC simulations and data.

Uncertainty	Yield change (±)
Luminosity	0.44%
$\sigma(ee \to \tau\tau)$	0.31%
Branching fractions (1 prong)	e: 0.22%
	μ: 0.22%
Branching fractions (3 prong)	3π: 0.57%
PID efficiency	e: 2%
	μ: 1%
	π: 3%
Bhabha contamination	0.2%
$q\bar{q}$ contamination (data)	0.1%
Tracking efficiency	Negligible
Detector modeling	Negligible
Beam energy	Negligible
Tau mass	Negligible

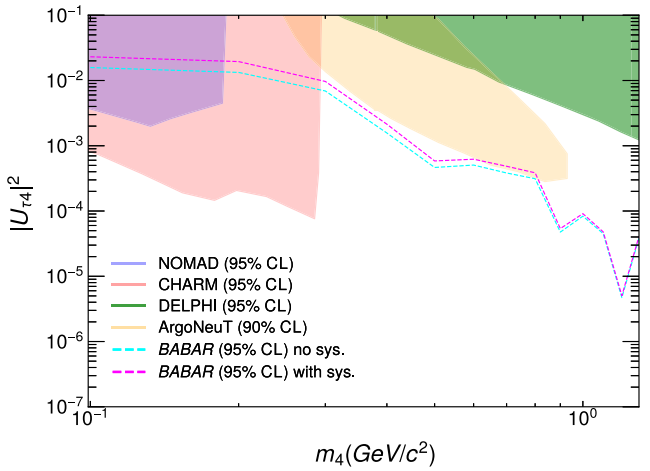

FIG. 10. Upper limits at 95% CL on $|U_{\tau 4}|^2$. The magenta line represents the result when uncertainties are included. The magenta line is expected to be a very conservative upper limit. Limits from Nomad [29], Charm [20], and Delphi [30] are also shown for reference. The recent ArgoNeuT result is also shown [31].

TABLE IV. Break down of upper limit on $|U_{\tau 4}|^2$ (95% CL) for each HNL mass hypothesis, with and without consideration of systematic uncertainty.

Mass [MeV/c^2]	No sys.	With sys.
100	1.58×10^{-2}	2.31×10^{-2}
200	1.33×10^{-2}	1.95×10^{-2}
300	6.91×10^{-3}	9.67×10^{-3}
400	1.57×10^{-3}	2.14×10^{-3}
500	4.65×10^{-4}	5.85×10^{-4}
600	5.06×10^{-4}	6.22×10^{-4}
700	3.82×10^{-4}	4.85×10^{-4}
800	3.12×10^{-4}	3.85×10^{-4}
900	4.70×10^{-5}	5.38×10^{-5}
1000	8.34×10^{-5}	9.11×10^{-5}
1100	4.49×10^{-5}	4.78×10^{-5}
1200	4.70×10^{-6}	5.04×10^{-6}
1300	3.85×10^{-5}	4.09×10^{-5}

Sec. IX B 2 that the effects of the modeling uncertainty were less apparent at higher HNL masses.

XI. CONCLUSIONS

The 95% C.L upper limits on $|U_{\tau 4}|^2$ obtained in this work for masses $100 < m_4 < 1300$ MeV$/c^2$ are shown in Fig. 10. Limits derived for the lower mass hypotheses are within the already excluded region, as expected since with this kinematic method the higher mass signals would produce the most signal/background discrimination, and, therefore, better limits. It should also be noted that the limits provided here are competitive with the current projections for experiments in the 5–10 year time frame in this mass range including those from Belle-II, FASER, and NA62 [2]. Looking further ahead, significant improvements are expected from the proposed facilities: the FCC-ee [49] and the ILC.

ACKNOWLEDGMENTS

We are grateful for the extraordinary contributions of our PEP-II colleagues in achieving the excellent luminosity and machine conditions that have made this work possible. The success of this project also relies critically on the expertise and dedication of the computing organizations that support *BABAR*. The collaborating institutions wish to thank SLAC for its support and the kind hospitality extended to them. We also wish to acknowledge the important contributions of J. Dorfan, W. Dunwoodie, and our deceased colleagues E. Gabathuler, W. Innes, D. W. G. S. Leith, A. Onuchin, G. Piredda, and R. F. Schwitters.

[1] J. Beacham *et al.*, J. Phys. G **47**, 010501 (2019).
[2] A. M. Abdullahi *et al.*, in 2022 Snowmass Summer Study (2022), arXiv:2203.08039.
[3] P. A. Zyla *et al.* (Particle Data Group), Prog. Theor. Exp. Phys. **2020**, 083C01 (2020).
[4] R. N. Mohapatra and G. Senjanovic, Phys. Rev. D **23**, 165 (1981).
[5] M. Fukugita and T. Yanagida, Phys. Rev. Lett. **89**, 131602 (2002).
[6] E. K. Akhmedov, V. A. Rubakov, and A. Y. Smirnov, Phys. Rev. Lett. **81**, 1359 (1998).
[7] S. Davidson, E. Nardi, and Y. Nir, Phys. Rep. **466**, 105 (2008).
[8] E. J. Chun *et al.*, Int. J. Mod. Phys. A **33**, 1842005 (2018).
[9] T. Asaka and M. Shaposhnikov, Phys. Lett. B **620**, 17 (2005).
[10] A. Boyarsky, O. Ruchayskiy, and M. Shaposhnikov, Annu. Rev. Nucl. Part. Sci. **59**, 191 (2009).
[11] T. Asaka, S. Blanchet, and M. Shaposhnikov, Phys. Lett. B **631**, 151 (2005).
[12] A. Palazzo, Mod. Phys. Lett. A **28**, 1330004 (2013).
[13] F. Kaether, W. Hampel, G. Heusser, J. Kiko, and T. Kirsten, Phys. Lett. B **685**, 47 (2010).
[14] J. N. Abdurashitov and Gothers (SAGE Collaboration), Phys. Rev. C **80**, 015807 (2009).
[15] G. Mention, M. Fechner, Th. Lasserre, Th. A. Mueller, D. Lhuillier, M. Cribier, and A. Letourneau, Phys. Rev. D **83**, 073006 (2011).
[16] A. Aguilar *et al.* (LSND Collaboration), Phys. Rev. D **64**, 112007 (2001).
[17] A. A. Aguilar-Arevalo *et al.* (MiniBooNE Collaboration), Phys. Rev. Lett. **110**, 161801 (2013).
[18] P. Abratenko *et al.* (MicroBooNE Collaboration), Phys. Rev. Lett. **128**, 241801 (2022).
[19] G. Bernardi *et al.*, Phys. Lett. B **203**, 332 (1988).
[20] J. Orloff, A. Rozanov, and C. Santoni, Phys. Lett. B **550**, 8 (2002).
[21] A. Vaitaitis *et al.* (NuTeV Collaboration), Phys. Rev. Lett. **83**, 4943 (1999).
[22] A. V. Artamonov *et al.* (E949 Collaboration), Phys. Rev. D **91**, 052001 (2015).
[23] M. Aoki *et al.* (PIENU Collaboration), Phys. Rev. D **84**, 052002 (2011).
[24] D. I. Britton *et al.*, Phys. Rev. D **46**, R885 (1992).
[25] J. Badier *et al.* (NA3 Collaboration), Z. Phys. C **31**, 341 (1986).
[26] E. Cortina Gil *et al.* (NA62 Collaboration), Phys. Lett. B **816**, 136259 (2021).
[27] P. Abratenko *et al.* (MicroBooNE Collaboration), arXiv: 2207.03840.
[28] P. Abratenko *et al.* (The MicroBooNE Collaboration), Phys. Rev. D **101**, 052001 (2020).
[29] P. Astier *et al.* (NOMAD Collaboration), Phys. Lett. B **506**, 27 (2001).
[30] P. Abreu *et al.* (DELPHI Collaboration), Z. Phys. C **74**, 57 (1997); **75**, 580(E) (1997).
[31] R. Acciarri *et al.* (ArgoNeuT Collaboration), Phys. Rev. Lett. **127**, 121801 (2021).
[32] J. C. Helo, S. Kovalenko, and I. Schmidt, Phys. Rev. D **84**, 053008 (2011).
[33] J. P. Lees *et al.* (*BABAR* Collaboration), Nucl. Instrum. Methods Phys. Res., Sect. A **726**, 203 (2013).
[34] B. Aubert *et al.* (*BABAR* Collaboration), Nucl. Instrum. Methods Phys. Res., Sect. A **479**, 1 (2002).
[35] B. Aubert *et al.* (*BABAR* Collaboration), Nucl. Instrum. Methods Phys. Res., Sect. A **729**, 615 (2013).
[36] A. Kobach and S. Dobbs, Phys. Rev. D **91**, 053006 (2015).
[37] R. Barate *et al.* (ALEPH Collaboration), Eur. Phys. J. C **2**, 395 (1998).
[38] S. Jadach, B. F. L. Ward, and Z. Was, Comput. Phys. Commun. **130**, 260 (2000).
[39] S. Jadach, J. H. Kuhn, and Z. Was, Comput. Phys. Commun. **64**, 275 (1990).

[40] D. J. Lange, Nucl. Instrum. Methods Phys. Res., Sect. A **462**, 152 (2001).
[41] T. Sjöstrand, Comput. Phys. Commun. **39**, 347 (1986).
[42] T. Sjöstrand and M. Bengtsson, Comput. Phys. Commun. **43**, 367 (1987).
[43] B. Ward, S. Jadach, and Z. Was, Nucl. Phys. B, Proc. Suppl. **116**, 73 (2003).
[44] S. Agostinelli *et al.* (GEANT4 Collaboration), Nucl. Instrum. Methods Phys. Res., Sect. A **506**, 250 (2003).
[45] Z. Lurie, Ph.D. thesis, University of British Columbia, 2002.
[46] J. S. Conway, in *PHYSTAT 2011* (CERN, Geneva, 2011), pp. 115–120.
[47] G. Cowan, K. Cranmer, E. Gross, and O. Vitells, Eur. Phys. J. C **71**, 1554 (2011); **73**, 2501(E) (2013).
[48] S. Algeri, J. Aalbers, K. Dundas Morå, and J. Conrad, Nat. Rev. Phys. **2**, 245 (2020).
[49] A. Blondel and P. Janot, Eur. Phys. J. Plus **137**, 92 (2020).